JGR Solid Earth

RESEARCH ARTICLE
10.1029/2024JB028977

Inhomogeneous Magnetization of Tyrrhenian Seamounts Revealed From Gravity and Magnetic Correlation Analysis

A. Barone[1], **M. Milano**[2], **and M. Fedi**[2]

[1]Institute for Electromagnetic Sensing of the Environment (IREA), National Research Council (CNR), Naples, Italy, [2]Department of Earth, Environment and Resources Sciences, University of Naples Federico II, Naples, Italy

Key Points:

- We may infer the rock magnetization of seamounts by the correlation analysis of gravity and magnetic anomalies
- The study of the potential field total gradients is particularly useful when the source has strong remanent magnetization
- We found inhomogeneous magnetization in the Palinuro, Marsili, Magnaghi and Vavilov seamounts, likely due to hydrothermal activity

Correspondence to:
M. Milano,
maurizio.milano@unina.it

Citation:
Barone, A., Milano, M., & Fedi, M. (2024). Inhomogeneous magnetization of Tyrrhenian seamounts revealed from gravity and magnetic correlation analysis. *Journal of Geophysical Research: Solid Earth*, *129*, e2024JB028977. https://doi.org/10.1029/2024JB028977

Received 21 FEB 2024
Accepted 19 AUG 2024

Author Contributions:
Conceptualization: A. Barone, M. Fedi
Data curation: A. Barone, M. Milano
Formal analysis: A. Barone
Methodology: A. Barone, M. Fedi
Project administration: M. Fedi
Supervision: M. Fedi
Validation: A. Barone, M. Milano, M. Fedi
Visualization: A. Barone, M. Milano
Writing – original draft: A. Barone, M. Milano, M. Fedi
Writing – review & editing: A. Barone, M. Milano, M. Fedi

Abstract We perform a joint analysis of gravity and magnetic data sets in the Tyrrhenian Sea region to infer the rock physical properties of several volcanic seamounts. We propose a moving-window application using Poisson's theorem, which relates the total gradient of the magnetic field to the total gradient of the first-order vertical derivative of the gravity field data. In volcanic environments, where strong intensity of remanent magnetization is expected, the total gradient of the magnetic field is particularly useful since it is almost independent on the direction of the total-magnetization. The moving-window approach resulted necessary due to the heterogeneous magnetization distribution of the volcanoes. First, we perform synthetic tests based on realistic seamount models which exhibit inhomogeneous magnetization intensity and orientation. Using the total gradients, we demonstrate that our approach can provide an appropriate magnetization-to-density ratio in different subareas of seamounts. The results of the correlation analysis for the Palinuro, Marsili, Vavilov, and Magnaghi seamounts provide interesting information on the variability of magnetization associated with different epochs of formation and demagnetization effects due to hydrothermal alteration processes.

Plain Language Summary We analyzed gravity and magnetic data sets to determine the rock properties of the main seamounts in Southern Tyrrhenian Sea. This study shows that the correlation analysis based on a window-by-window approach is an efficient tool for studying potential field anomalies in areas where inhomogeneous distribution of magnetization is expected. We also show that, by studying the total gradients of the magnetic field and the first order vertical derivative of the gravity field, the correlation analysis is almost insensitive to the direction of the remanent magnetization. We obtain interesting information on the variability in magnetization for each seamount and identify possible areas of demagnetization due to hydrothermal alteration processes.

1. Introduction

The study of the complex geological architecture of the Tyrrhenian Sea back-arc basin is of great interest for understanding the processes involved in the geodynamics of the Afro-European plates. Extensional movements and seafloor spreading have had a great impact on the present-day structural setting of this region, as they led to the formation of small ocean basins and numerous submarine volcanic districts (e.g., Carminati et al., 1998; Faccenna et al., 2003; Malinverno & Ryan, 1986).

Geophysical measurements have proved to be crucial for investigating the structural framework of the deep and shallow crust of the Tyrrhenian Sea (e.g., Contrucci et al., 2001; Contrucci et al., 2005; Finetti, 2005; Panza et al., 2007; Prada et al., 2014). In particular, potential field investigations represent non-invasive approaches to explore large areas with high resolution and allow effective modeling of subsurface sources in terms of density and magnetization distributions (e.g., Barbosa & Silva, 2011; Blakely, 1996; Cella et al., 2008; Florio et al., 2021; Hinze et al., 2013; Kelemework et al., 2021; Milano et al., 2020; Olesen et al., 2010; Zuo et al., 2019). These methods are particularly useful for remotely studying areas that are difficult to access, where other geophysical techniques might be too expensive and where in-situ sample collection is difficult, such as regions characterized by submarine volcanic activity. In this scenario, the Tyrrhenian Sea hosts numerous submarine mountains and a complex pattern of potential field's anomalies (e.g., Cella et al., 2008). As a result, in last decades potential fields have been widely used as alternative and complementary methods to other geophysical techniques, helping to improve knowledge of Tyrrhenian volcanic edifices and the structural evolution of the entire basin (e.g., Caratori Tontini et al., 2009; Cella et al., 1998; Cocchi et al., 2023; De Ritis et al., 2010; Faggioni et al., 1995; Fedi et al., 1994; Florio et al., 2011; Savelli & Schreider, 1991).

Inverse techniques are commonly used to model potential field data. However, to reduce the inherent ambiguity of potential field problems, we need a priori information consisting of direct information on the source property or on general features of the source model, such as compactness or other (e.g., Liu et al., 2018). Here, we use a different method for seamounts investigation that is the correlation analysis between the magnetic and gravity anomaly fields (e.g., von Frese et al., 1982; von Frese et al., 1997). Obviously, also this method requires a priori information, consisting in assuming the same volume for both the potential field problems and, in our case, to estimate the magnetization intensity contrast assuming the density contrast. While the volume requirement is discussed in this paper (Section 3.1), the density contrast may be reasonably considered constant for the seamounts. It follows that a rapid estimate of the average source density can be performed from the correlation analysis between topography and gravity data (e.g., Nettleton, 1939), assuming that the gravity anomaly is mainly related to the shape of a seamount and that the rock density is fairly homogeneous; conversely, similar assumption is not valid for the seamount magnetic properties. For instance, numerous studies have proved that the Tyrrhenian seamounts are affected by hydrothermal activity, which produces mineral alteration and permanent effects on rocks magnetization (e.g., Caratori Tontini et al., 2014; Cocchi et al., 2021; Ligi et al., 2014; Loreto et al., 2019). In addition, volcanic activity, that often extends over time, can induce significant variability of the remanent magnetization effect of mafic rocks. Consequently, the associated magnetic anomalies present a more complex behavior than the gravity ones, which are certainly more related to the morphology of the seamount. So, the correlation method between potential field anomalies seems appropriate to give a first estimate of the magnetization contrast, useful also for further investigations involving data inversion (e.g., Milano et al., 2021).

This approach, based on the properties of Poisson's theorem (Blakely, 1996), allow the determination of the Magnetization-to-Density Ratio (MDR) of potential field sources. The theorem consists of the relationship between the directional derivatives of magnetic and gravity potentials produced by uniform and homogeneous source distributions of magnetization and density (Garland, 1951). The Poisson's analysis has been successfully applied for several purposes, including, for example, the evaluation of the source physical features (Alencar de Matos & Mendonça, 2020; Garland, 1951; Kanasewich & Agarwal, 1970; Mendonca, 2004; Milano et al., 2021) or of the source magnetization direction (Cordell & Taylor, 1971; Ross & Lavin, 1966).

In the Tyrrhenian Sea, De Ritis et al. (2010) performed a correlation analysis of first order vertical derivative of gravity and reduced-to-pole (RTP) magnetic data. However, on a regional basis, they found a nearly zero correlation coefficient and concluded that there is a lack of correlative anomaly features. At a smaller scale, Fedi et al. (1994) studied the Magnaghi seamount with the Poisson's theorem applied to pseudogravity and gravity fields and magnetic data inversion, concluding that the magnetization distribution is complex, while the density distribution may be assumed as nearly homogeneous.

In this scenario, we propose a study of the magnetization of the Tyrrhenian seamounts through a moving-window correlation analysis (Chandler et al., 1981) by involving the total gradient transformations of potential field data (Doo et al., 2009). This transformation is very useful for the magnetic data since it is relatively unsensitive to the remanent magnetization direction (Nabighian, 1972; Stavrev & Gerovska, 2000). In fact, when remanent magnetization is strong, the RTP transformation is likely to fail and cannot be safely used for removing the dipolar effects of magnetic anomalies. On the other hand, the window-based analysis is very useful in the case of a complex distribution of magnetization, as it allows the inhomogeneity of the seamount to be determined.

We start from formulating the Poisson's relation in terms of total gradients of the magnetic anomalies and first order vertical derivative of gravity data. We test our approach on synthetic data relative to a source with uniform density distribution, inhomogeneous magnetic properties and strong remanent magnetization.

We then conduct the proposed analysis on the magnetic and free-air gravity anomalies of four different seamounts in the Southern Tyrrhenian Sea: Palinuro, Marsili, Vavilov and Magnaghi. The seamounts magnetization intensities are computed from the estimated MDR by assuming the average rock densities obtained through Nettleton's method (Nettleton, 1939).

2. Geological Setting

The Tyrrhenian Sea (Figure 1a) is a back-arc basin developed as consequence of the W-to-NW subduction of the African lithospheric plate under the Apennines, Calabrian Arc, and Maghrebides orogenic belts (Faccenna et al., 2001; Gvirtzman & Nur, 2001; Malinverno & Ryan, 1986; Patacca et al., 1990; Patacca & Scandone, 2001;

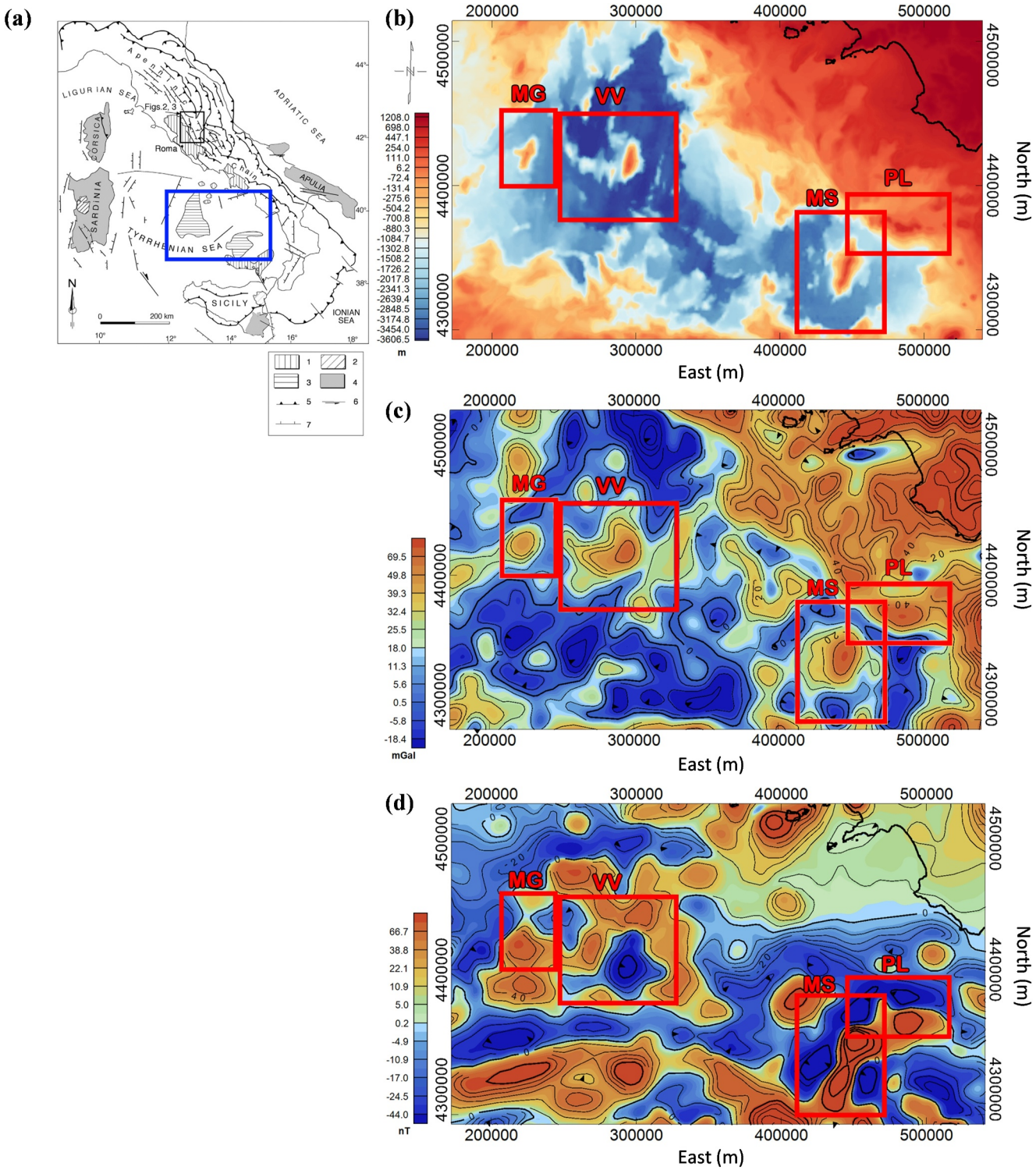

Figure 1. (a) Sketch map with the main structural and geological units (modified after Mancini & Cavinato, 2009; Cavinato & Celles, 1999): 1, subduction-related and high-K volcanic rocks; 2, extension-related volcanic rocks; 3, oceanic crust; 4, foreland areas; 5, subsurface and surface thrust front; 6, strike-slip fault; 7, extensional fault. (b) Bathymetric, (c) free-air and (d) aeromagnetic field maps of Southern Tyrrhenian Sea (blue box in subpanel a). The red squares indicate, from East to West, the location of Palinuro (PL), Marsili (MS), Vavilov (VV) and Magnaghi (MG) seamounts.

Royden, 1988). Since the Tortonian (11.6−7.2 Ma), the Southern Tyrrhenian basin evolved with an eastward retreat of the subduction system with a rate of about 5–6 cm/yr (Doglioni et al., 1994; Patacca et al., 1990). Rollback processes involving the heavy Ionian oceanic lithosphere favored E–W and N–S extension and the formation of intra-slope basins and the Vavilov back-arc basin (Doglioni et al., 2004). In middle Pliocene, new rifting events took place and E-W to NE–SW trending normal faulting affected the coastal morphology of Northern Sicily (e.g., Faccenna et al., 1997; Patacca et al., 1990; Royden, 1988). Later, throughout the late Pliocene-Quaternary, the crustal thinning and oceanic crustal accretion moved southeastward and culminated with the development of seamounts and seafloor spreading. These processes let the formation of the Marsili back-arc basin and the migration of the volcanism to the Aeolian arc, which gave the present-day configuration of the Southern Tyrrhenian region (e.g., Kastens et al., 1988; Ligi et al., 2014).

Research on hydrothermal activity in the Tyrrhenian Sea contributes to our understanding of the geological processes associated with submarine volcanic systems. It has also implications for the study of deep-sea ecosystems and mineral resources. Hydrothermal activity in Southern Tyrrhenian Sea (Figure 1b) has been widely documented by the presence of a wide range of oxyhydroxide and sulfide deposits (e.g., Bonatti et al., 1972; Dekov et al., 2009; Dekov & Savelli, 2004; Gamberi et al., 1997). As a result, mineralogical, chemical, and textural alterations have been observed due to the interaction between hot fluids and the volcanic rocks (e.g., Beccaluva et al., 1990; Trua et al., 2002). However, further explorations and studies are needed to fully comprehend the extent and dynamics of Tyrrhenian Sea seamounts and their hydrothermal activity.

The Palinuro volcanic complex (PL in Figure 1) is characterized by an almost E-W linear trend, whose structural origin is still debated (e.g., Chiarabba et al., 2008; Colantoni et al., 1981; Del Ben et al., 2008; Milano et al., 2012; Milia et al., 2009). The shallowest portion of the volcanic edifice is located at about 90 m b.s.l. and has a lateral extension of about 70 by 20 km^2, with its southern flank merging with the Marsili basin. The Palinuro seamount is mostly constituted of rocks with basalt-andesite compositions (Trua et al., 2004) and is also characterized by a collapsed caldera structure in the western region.

The Marsili seamount (MS in Figure 1) consists of an imposing volcanic edifice rising for approximately 3,000 m from the basin seafloor, with lateral extension of about 70 by 30 km^2. It was formed during the emplacement of oceanic-type basalts (Kastens et al., 1988; Marani & Trua, 2002) following the extensional tectonics. Its formation was interpreted as due to strong magma upwelling from the subducting Ionian slab (e.g., Marani & Trua, 2002), or to the change from extensional to compressive tectonics with its emplacement on top of a relict back arc basin (e.g., Ventura et al., 2013).

The Vavilov volcano (VV in Figure 1), located about 180 km SW of Vesuvius, is a large volcanic structure mostly consisting of tholeiitic to alkali basalts (Robin et al., 1987) of Late Pliocene age (Kastens et al., 1988; Savelli, 2002). Its formation occurred during the oceanization of the Vavilov basin about 3 Ma (Kastens et al., 1988). The volcano manifests a visible asymmetry consisting of an irregular topography of the eastern flank and a smooth and steep western flank; one possible cause involves the collapse of a portion of the seamount.

The Magnaghi seamount (MG in Figure 1) is a large elliptical volcanic structure extending NNE–SSW from a depth of about 2,800 m to about 1,880 m b.s.l and classified as a giant fissural volcano (e.g., Sartori et al., 2004). Its lava products mostly consist of alkaline to weakly alkaline basaltic composition with a MORB/OIB affinity (Cocchi et al., 2008; Robin et al., 1987; Savelli, 1988; Serri et al., 2001). K/Ar dating of these samples analysis of the Magnaghi seamount suggested ages between 2.7 and 3.1 Ma, which took place during normal and reverse polarity periods C2An.1n-C2An.2r (Cocchi et al., 2008; Schreider, 1993).

2.1. Potential Field Data Sets

The potential field data sets used in this work derive from the gravity and aeromagnetic maps of Italy (AGIP, 1981; Carrozzo, 1981; Carrozzo et al., 1981; Chiappini et al., 2000; ISPRA et al., 2009). The gravity measurements were collected by the Osservatorio Geofisico Sperimentale (OGS) with a 3 km track spacing and an accuracy of about ±3 mGal (Gantar et al., 1968; Morelli et al., 1975a, 1975b). These data have been supplemented with marine satellite altimetry measurements obtained by the GEOSAT and ERS-1 missions (Sandwell & Smith, 1997). The aeromagnetic survey was carried out between 1977 and 1979 by the Italian oil company (AGIP, now ENI) covering both the onshore and offshore areas of the Italian territory (Chiappini et al., 2000). In particular, the Tyrrhenian Sea has been covered by eight separate surveys at a constant

observation level of 1,463 m a.s.l. (e.g., Cassano et al., 1986a, Cassano et al., 1986a). The data were acquired using a cesium magnetometer with an average sampling step of 100 m along a set of parallel track-line NE–SW with a spacing of 2–5 km, intersected by orthogonal control tie-lines spaced about 5–10 km (Caratori Tontini et al., 2004).

Here, we use a limited portion of the free-air gravity and aeromagnetic data sets covering the main basins of the Southern Tyrrhenian Sea and the related seamounts, with a 2 km data spacing. We show the analyzed maps of the potential field anomalies in Figures 1c and 1d; we can clearly observe the dominant effect of the volcanic edifices on the gravity and magnetic features of the region. The free-air gravity anomalies are visibly associated with the density contrast between the dense volcanic rocks and the surrounding water column. The shape of these anomalies, in fact, strongly correlates with the sharp morphology of the seamounts and of the intermediate Tyrrhenian Sea basins. The aeromagnetic map has a more complex behavior (e.g., Cella et al., 1998; Cella et al., 2008; Florio et al., 2022). More specifically, the aeromagnetic map shows distinct magnetic signatures in the Palinuro volcanic area, indicating a difference in the rock magnetization of the volcanic edifice. According to Caratori Tontini et al. (2009), we may find evidence of inhomogeneous rocks magnetization in the Palinuro seamount between the less magnetized eastern area and the intensely magnetized central and western regions. Areas with low magnetic signatures have been also interpreted in correspondence with hydrothermal deposits and alteration of the volcanic rocks (e.g., Caratori Tontini et al., 2009; Caratori Tontini et al., 2010; Colantoni et al., 1981; Minniti & Bonavia, 1984). Above the Marsili seamount, the magnetic field map shows two distinct anomalies corresponding to the southern and northern tips of the volcanic edifice.

The Vavilov seamount presents a more complex magnetic field with anomalies associated with the different spreading phases of the basin (Savelli & Schreider, 1991). The most evident magnetic signature is represented by an intense anomaly with reverse polarity, which is consistent with the estimated age and rock magnetization direction (Robin et al., 1987). Reversely magnetized rocks have been found West, North and East of the volcanic edifice, while normally magnetized rocks characterize the areas all around the basin (e.g., Savelli & Ligi, 2017). Finally, the aeromagnetic field above the Magnaghi seamount shows an intense and tilted magnetic anomaly with the high along the western flank of the volcano and the low north-eastward (Cella et al., 2008).

3. Method

Consider a body source with homogeneous density contrast $\Delta\rho$ and homogeneous magnetization intensity contrast ΔJ and uniform direction $\mathbf{t}$. Poisson showed that its magnetic potential V_m and Newtonian gravity potential ϕ_g are related as (Blakely, 1996):

$$V_m = \frac{\mu_0}{4\pi\gamma}\frac{\Delta J}{\Delta\rho}\frac{\partial}{\partial \mathbf{t}}\phi_g \tag{1}$$

where $\Delta J/\Delta\rho$ is the Poisson's ratio, here called MDR, μ_0 and γ are the magnetic and gravitational constants, respectively.

A first and more practical form of the Poisson's relation can be defined between the pseudo-gravity magnetic field (V_g) and the vertical component of the gravity field (g_z). In this case Equation 1 becomes:

$$V_g = \frac{\mu_0}{4\pi\gamma}\frac{\Delta J}{\Delta\rho}g_z \tag{2}$$

A second and commonly used form of Poisson's relation can be obtained by deriving both members of Equation 2 along the z-direction, as follows:

$$\Delta T_{rp} = \frac{\mu_0}{4\pi\gamma}\frac{\Delta J}{\Delta\rho}g_{zz} \tag{3}$$

which relates the RTP transform of magnetic field (ΔT_{rp}) and the first order vertical derivative of the gravity field (g_{zz}); we can achieve other valid relations by further increasing the differentiation order of both members of Equation 3 (e.g., Milano et al., 2021). Both Equations 2 and 3 are obtained by setting $t = z$, which implicitly

assumes that the source is mainly induced-only magnetized. On the other hand, if the source remanent magnetization intensity is not negligible, information about the magnetization direction is required, which however is rarely available.

For this reason, we use an alternative form of the Poisson's relation based on the total magnetic gradient ($|\nabla T|$) which is defined as $|\nabla T| = \sqrt{\left(\frac{\partial T}{\partial x}\right)^2 + \left(\frac{\partial T}{\partial y}\right)^2 + \left(\frac{\partial T}{\partial z}\right)^2}$ (Doo et al., 2009; Milano et al., 2019; Nabighian, 1972; Stavrev & Gerovska, 2000). Specifically, according to Roest et al. (1992), this transformation, in a 3D problem, is almost independent of the direction of source body magnetization and the direction of the geomagnetic field. We thus can write the Poisson's relation in the following form:

$$|\nabla T| \cong \frac{\mu_0}{4\pi\gamma}\frac{\Delta J}{\Delta\rho}|\nabla g_{zz}| \tag{4}$$

where $|\nabla g_{zz}|$ is the total gradient of the first order vertical derivative of the measured gravity field. The advantage of using Equation 4 is that we can compute the MDR regardless of the intensity of the source remanent magnetization component since the total gradient evaluation does not require this information.

3.1. Estimation of the Source Physical Properties

The Poisson's relation states that we can easily infer the source physical properties when the magnetic potential is proportional to the component of gravity attraction in the direction of magnetization (Blakely, 1996), which implies that the source boundaries of the gravity and magnetic anomalies source are the same and the magnetization and density are uniform. Nevertheless, according to Blakely (1996), Equation 1 is still valid in the case of no uniform distribution of J and ρ by considering both the gravity and magnetic sources as composed of elementary volumes. To do that, in this study, we perform the Poisson's analysis by using the moving-window correlation approach (Chandler et al., 1981, 1991) that is particularly suitable to study multisource cases.

The approach is based on a least squares linear regression between magnetic and gravity data sets within a moving-window. Without loss of generality, we can use the following linear equation to express any chosen form of the Poisson's relation:

$$\Theta = \mathrm{MDR}\cdot\Gamma + K \tag{5}$$

where Θ and Γ are any proper transformations for the Poisson's analysis of the magnetic and gravity data sets respectively, MDR is the slope coefficient of the linear relation, and K is the intercept. K should be approximately constant, as it should represent contributions on a regional scale with much longer wavelengths than those of the analyzed anomaly, or account for variations in the base level of the anomaly. In this view, the approach evaluates the coefficients of the magnetic and gravimetric data sets linear regression for each window.

Specifically, we calculate the correlation (R), K and, following Chandler et al. (1981), we estimate an average MDR (slope parameter) in the areas where R is high and K is stable. Finally, to infer the source magnetization, we multiply the MDR values, obtained at each window, for the density contrast, which is assumed constant for each volcanic structure. We specify that the moving-window step is here considered to be equal to the sampling step of the analyzed data set (2 km).

The density value of the seamount rocks is here estimated using to the Nettleton's method (Nettleton, 1939). This approach is based on a correlation analysis between the topographic/bathymetric surface and the related Bouguer anomaly estimated assuming a range of different ρ values. Hence, we find as correct ρ the value that ensures the lowest correlation between the calculated Bouguer anomaly and bathymetry. The obtained ρ is then transformed into $\Delta\rho$ by considering the contrast between the volcanic edifice and the surrounding seawater, that is about 1,000 kg/m^3. Similarly, we may retrieve the J distribution from the evaluated ΔJ by taking into account that the seawater magnetization is equal to 0 A/m, so implying $\Delta J = J$.

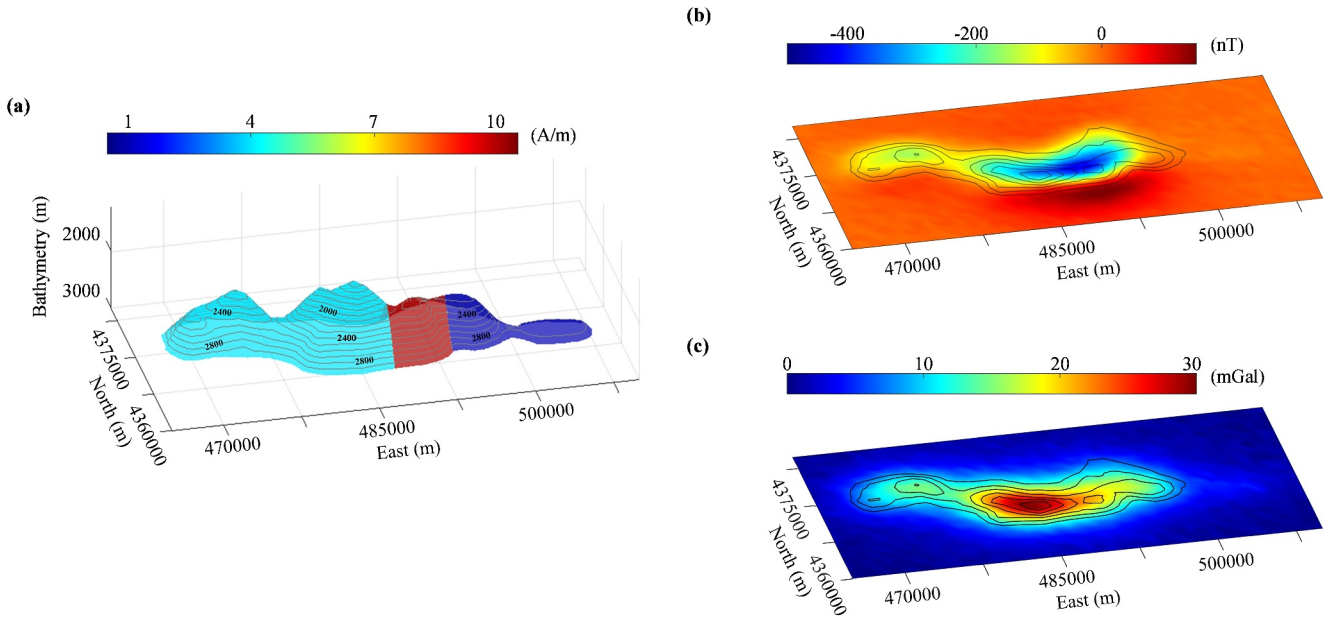

Figure 2. Simulated scenario. (a) ΔJ source distribution of the simulated seamount; the gray lines are the contours of the seamount bathymetry; the vertical scale is exaggerated. The $\Delta\rho$ of the model is 1,500 kg/m^3. (b) Magnetic and (c) gravity anomalous fields produced by the body source in (a). Both potential fields data sets are contaminated with a 5% random Gaussian noise.

3.2. Synthetic Modeling

Here, we test the method in the case of the inhomogeneously magnetized seamount. To do this, we use the bathymetry of the Palinuro seamount to generate a geometrically irregular model characterized by three regions with different magnetization intensities. The source $\Delta\rho$ is fixed to 1,500 kg/m^3, while total ΔJ varies, from West to East, from 4 to 10 and 1 A/m (Figure 2a), and we assume a Koenigsberger ratio $Q = 40$, according to the average value of rock samples from the Tyrrhenian seamounts having strong remanent magnetization (Faggioni et al., 1995). We set the induced magnetic field with the average values of declination (D_I) and inclination (I_I) of the Tyrrhenian area, that is, $D_I = 3°$ and $I_I = 57°$, while $D_R = -10°$ and $I_R = -30°$ are the declination and inclination of the source remanent magnetization. We thus estimated the gravity and magnetic responses using the Parker (1972) algorithm. To better simulate real-world conditions, we included a zero-mean random Gaussian noise equal to 5% of the maximum amplitude in each data set. In Figures 2b and 2c we show the forward gravity and magnetic responses of the above model computed at the sea level with a 2 km data spacing. We then apply upward continuation procedure in order to reduce the high-frequency noise affecting both the data sets. The measurements level is therefore changed to an altitude of 1,500 m a.s.l.

We consider now three different cases (Figure 3):

1. The first is based on the most used form of the Poisson's analysis between the RTP magnetic field (Figure 3a) and the first order vertical derivative of the gravity field (Figure 3d), assuming that we know the correct values of D_R and I_R. However, in the real world, little information is available on the remanent magnetization of the rocks. Moreover, the complexity of the magnetic property distribution, as simulated here, makes even more challenging the local knowledge of this information;
2. The second is when we have no information about remanent magnetization and the RTP transformation is performed assuming that $D_R = D_I$ and $I_R = I_I$ (Figure 3b); this approach leads to obvious error in the calculation of the RTP magnetic anomaly;
3. The third case is using the Poisson's analysis based on the total gradients of the magnetic field (Figure 3c) and the first vertical derivative of the gravity field (Figure 3e).

For all the cases, we use a small 4×4 km^2 window. Although the suggested size should be between 0.5 and 1 times the half-width of the anomaly wavelength of primary interest (Chandler et al., 1981), we choose the smallest

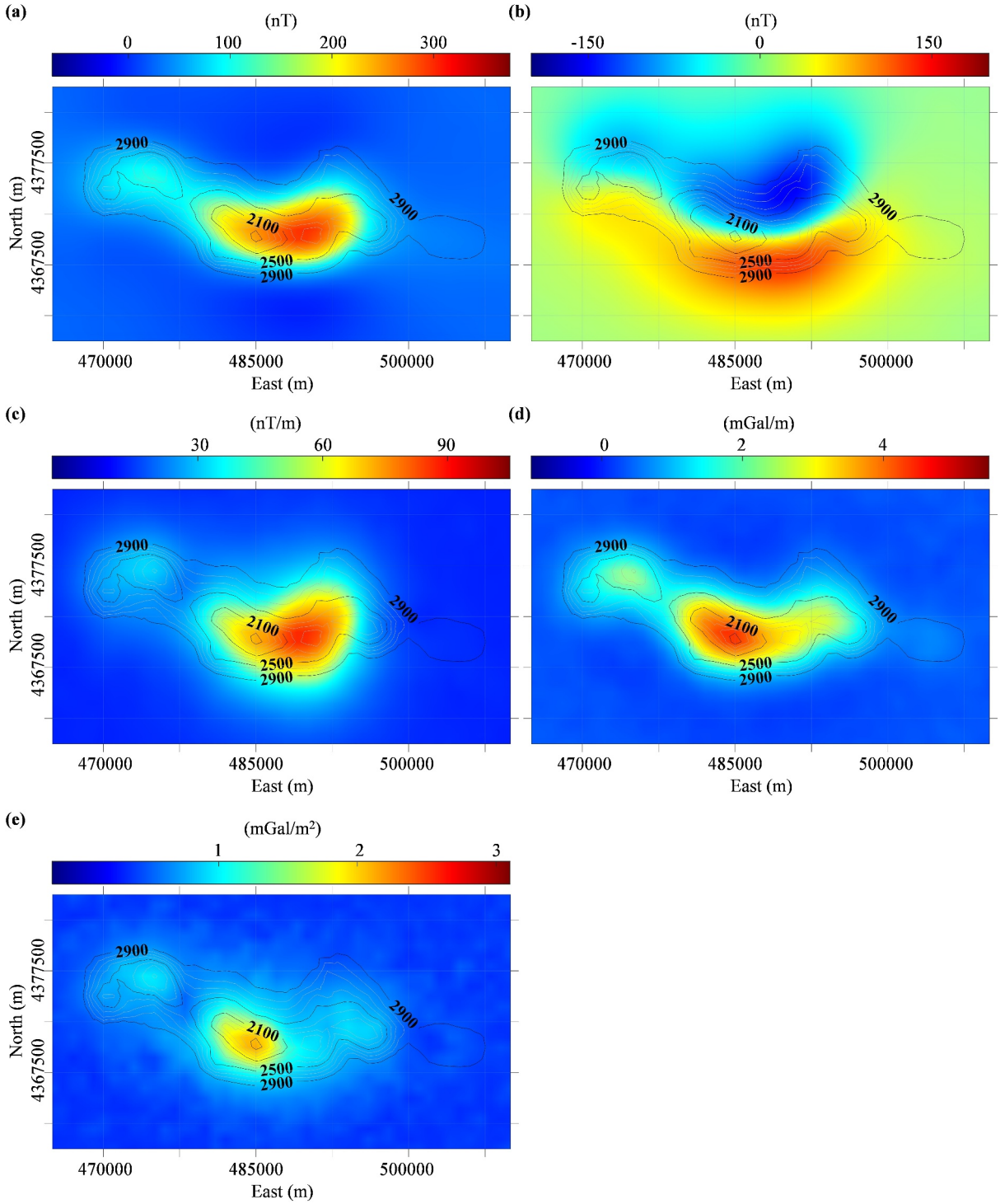

Figure 3. Synthetic model example. RTP magnetic field (a) computed using the correct D_R and I_R values and (b) assuming $D_R = D_I$ and $I_R = I_I$. (c) Total gradient of the magnetic field. (d) First order vertical derivative of the gravity field and (e) its total gradient transformation. The black and gray contour lines represent the simulated seamount bathymetry. Field transformations are computed starting from noisy data sets referred to a measurements level with 1,500 m a.s.l. of altitude, as described in the main text.

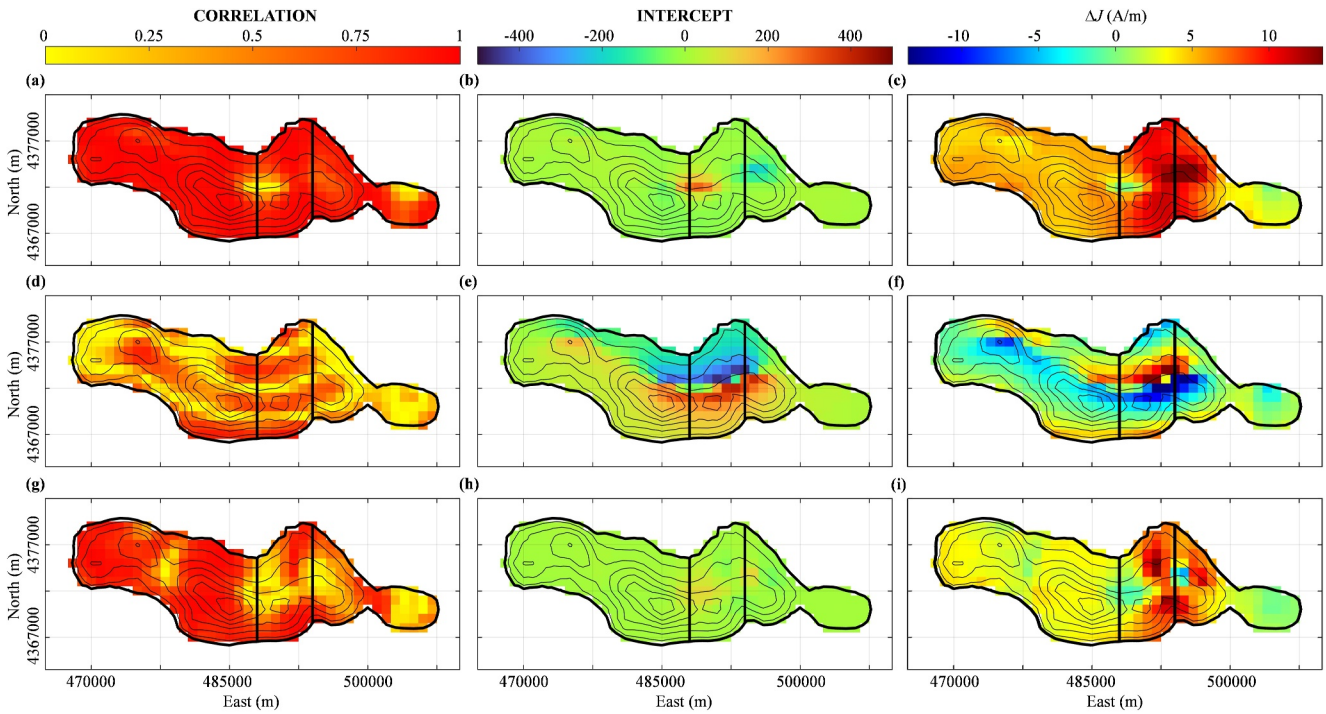

Figure 4. Results of the simulated Poisson's analyses. Evaluated distribution of the (a–d–g) correlation (R), (b–e–h) intercept (K) coefficients and (c–f–i) ΔJ parameter for the three different simulated scenario, respectively. Black lines delineate the three areas with different ΔJ distribution.

window size to simulate real case analysis where several inhomogeneities cause anomalous and interfering fields with variable wavelength.

In Figure 4 we provide the maps of R and K coefficients and ΔJ distribution within the simulated seamount for the three different cases. The magnetization is estimated in the areas where $R > 0.7$, which, according to Fedi et al. (1994), is a suitable lower boundary for this kind of analysis. In the following, we describe the main results obtained for each case and provide the magnetization estimates with their uncertainty σ. In particular, σ is calculated from the estimates of ΔJ in each different sector, where $R > 0.7$.

The results show that:

- In the first case, using the correct RTP data we yield three major areas with high correlation (Figure 4a) separated by two minima; in these sectors, K (in nT) is stable (Figure 4b) and the slope coefficient can be used to estimate the ΔJ distribution (Figure 4c); we estimate a mean magnetization contrast $\overline{\Delta J}$ about 5.04 A/m with standard deviation $\sigma = 0.75$ A/m for the western subpart, $\overline{\Delta J} = 9.88$ A/m with $\sigma = 1.96$ A/m for the central area, and $\overline{\Delta J} = 2.39$ A/m with $\sigma = 1.16$ A/m for the eastern zone;
- In the second scenario, the wrong assumption used for the computation of the RTP magnetic field yields a low R, as observed in the map in Figure 4d; also, K (Figure 4e) assumes variable values and the identification of the source inhomogeneities is unclear; as a result, the estimated ΔJ distribution (Figure 4f) mostly consists in unrealistic negative values; we only observe highly correlated areas for the western sector, where $\overline{\Delta J} = 4.33$ A/m with $\sigma = 3.75$ A/m, and for the central zone, with estimate of $\overline{\Delta J} = 5.15$ A/m with $\sigma = 7.65$ A/m;
- In the last case, the analysis between the total gradients of the gravity and magnetic data shows a correlation map (Figure 4g) characterized by three main areas with high values corresponding with stable K (in nT/m) (Figure 4h); the inferred $\overline{\Delta J}$ is about 3.28 A/m with $\sigma = 0.45$ A/m for the western sector, 9.62 A/m with $\sigma = 2.53$ A/m for the central area, and 0.94 A/m with $\sigma = 0.23$ A/m for the eastern zone.

These results show that our approach is well suitable for complex magnetic source distributions, regardless the disturbing noise effect. In fact, we observe that, in the last case, it is possible to infer the correct magnetization distribution with low uncertainty, without providing information about the source magnetization direction. On the other hand, we also note that the moving-window approach may have limitations in the interference regions

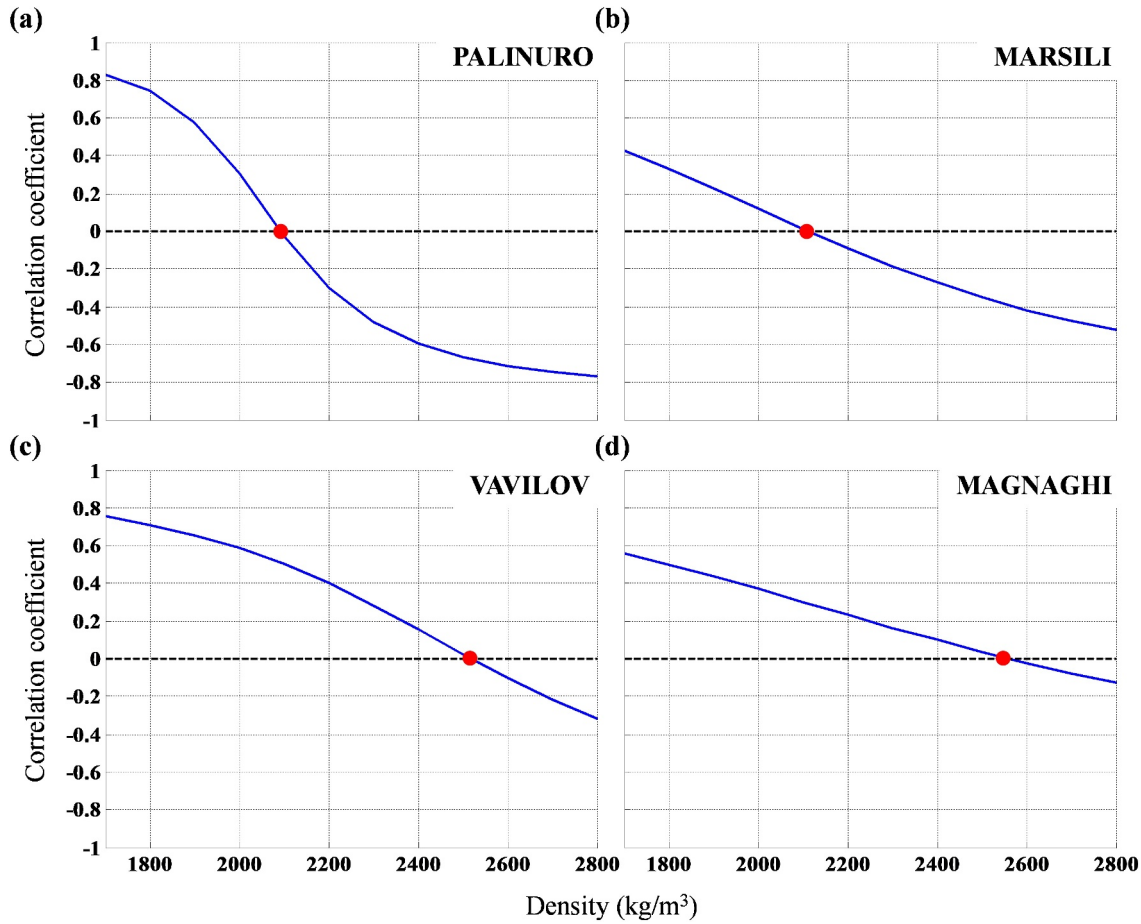

Figure 5. Density estimation for Tyrrhenian seamounts. Correlation analysis between bathymetry and Bouguer anomaly computed by considering different density values for (a) Palinuro, (b) Marsili, (c) Vavilov and (d) Magnaghi seamounts. The black dashed lines highlight the zero correlation line, while the red dots represent the retrieved seamount density.

among anomalies of nearby sources. In fact, according to Chandler et al. (1981), the results show two positive and negative peaks of the slope coefficient in the transition areas among rocks with different magnetization (Figures 4c, 4f, and 4i). This effect therefore prevents a correct estimation of the MDR and interpretation must be restricted to areas outside the interference regions. Nevertheless, we also note that the use of the total gradient favors the enhancement of the signal on a local scale, thus reducing such disturbing effect.

4. Results

We here discuss the results of the proposed analysis in the Tyrrhenian region to characterize the physical properties of the Palinuro, Marsili, Vavilov and Magnaghi seamounts.

4.1. Density Estimation for Tyrrhenian Seamounts

First, we use the Nettleton's method (Nettleton, 1939) for a fast characterization of the representative seamount densities. Specifically, for each seamount, we calculate the Bouguer anomaly from the free-air gravity for $1{,}700 < \rho < 2{,}700$ kg/m^3. Considering the contrast with the seawater column ($\rho_w \sim 1{,}000$ kg/m^3) above the volcanic structures, we actually use a density contrast ranging from 700 to 1,700 kg/m^3. We then compute their correlation coefficient with respect to the seamount bathymetry and select those providing to the lowest correlation values.

In Figure 5 we show the average values obtained for the seamounts: $\rho = 2{,}100$ kg/m^3 for Palinuro (Figure 5a); $\rho = 2{,}100$ kg/m^3 for Marsili (Figure 5b); $\rho = 2{,}500$ kg/m^3 for Vavilov (Figure 5c) and $\rho = 2{,}600$ kg/m^3 for

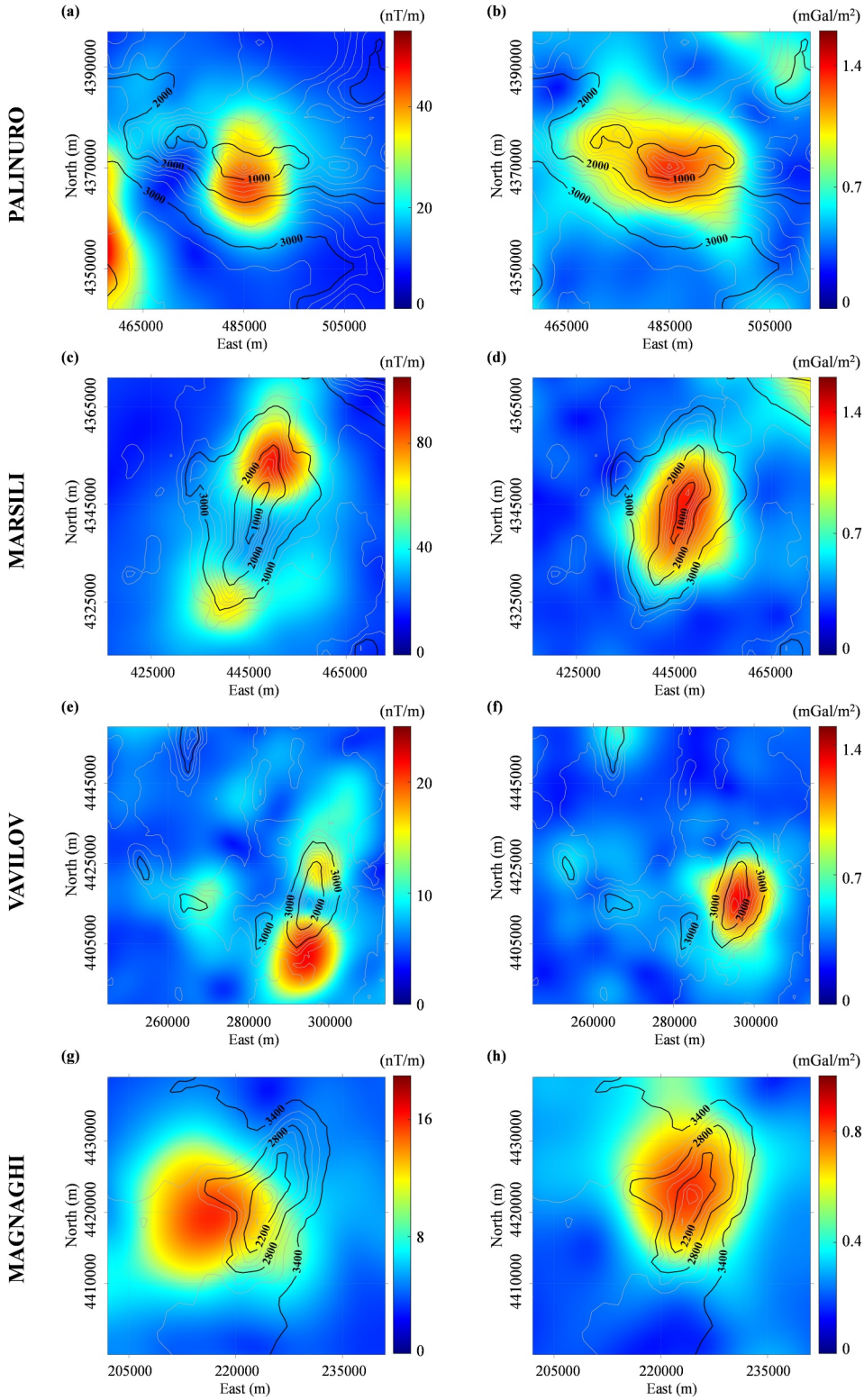

Figure 6. Total gradient maps (a) of the magnetic field and (b) of the first order vertical derivative of the gravity field at Palinuro, (c–d) Marsili, (e–f) Vavilov and (g–h) Magnaghi seamounts. The black and gray contour lines represent the seamounts bathymetry.

Magnaghi (Figure 5d). For the Marsili seamount we confirm the density value estimated by Fedi (1997) with a totally different approach.

4.2. Magnetization Estimation for Tyrrhenian Seamounts

To perform the Poisson's analysis to the four selected Tyrrhenian seamounts, we first compute the total gradients of the potential field data sets shown in Figures 1c and 1d. Figure 6 shows the total gradient maps of the magnetic field and of the first order vertical derivative of the gravity data for Palinuro (Figures 6a and 6b), Marsili (Figures 6c and 6d), Vavilov (Figures 6e and 6f) and Magnaghi (Figures 6g and 6h) seamounts.

In Figure 7, we show the maps of the correlation (Figures 7a, 7d, 7g, and 7j), intercept (Figures 7b, 7e, 7h, and 7k) and slope coefficients obtained using a 4×4 km^2 moving-window that are multiplied by the above indicated average $\Delta\rho$ in order to map the ΔJ distribution of each seamount (Figures 7c, 7f, 7i, and 7l).

The results show that:

- Palinuro seamount (Figures 7a–7c): we observe at least three highly correlated areas (Figure 7a) with stable K values (Figure 7b) around the seamount summit, where we evaluate a maximum $\Delta J \sim 10$ A/m for the northern central, eastern and southern regions of the seamount ("A," "B," "C" in Figure 7c); moving eastward, we observe a rapid decrease of rock magnetization reaching very low values above the eastern crest of the seamount ("D" in Figure 7c). On the north-westward area, we also note the typical interference effect similar to what discussed in the previous synthetic case ("E" in Figure 7c). Here, we observe coupled negative and positive peaks that preclude the estimation of the magnetization in this restricted area.
- Marsili seamount (Figures 7d–7f): we observe zones with high correlation (Figure 7d) and stable K (Figure 7e) coefficients mostly located in the lateral portions of the seamount. In Figure 7f, we find mostly high rock magnetization reaching values of about 15–20 A/m at the northern and southernmost sub-portions of the seamount ("F," "G" in Figure 7f). We also note interference effects which mostly interest the central area of the volcanic edifice ("H" in Figure 7f).
- Vavilov seamount (Figures 7g–7i): the maps show several small highly correlated areas (Figure 7g) characterized by stable K values (Figure 7h), negative ("K" in Figure 7i) and positive ΔJ distribution (Figure 7i) both at and around the volcanic edifice; specifically, a maximum $\Delta J \sim 2$ A/m value characterizes the north-western sector of the seamount ("J" in Figure 7i), while higher values occur in the outwards basin ("I" in Figure 7i). In general, in contrast with previous cases, we infer very low magnetization values characterizing the main volcanic edifice.
- Magnaghi seamount (Figures 7j–7l): we observe at least three areas with high R (Figure 7j), stable K (Figure 7k) and positive ΔJ at its Northern, Southern and Western subparts ("M," "N," "O" in Figure 7l), with maximum $\Delta J \sim 5$ A/m; in the central region, we also observe negative ΔJ values which can be again associated with the effect of interference among gravity and magnetic anomalies ("P" in Figure 7l).

5. Discussion

Our approach allows to overcome some limitations usually encountered in the Poisson's analysis, such as the not uniform orientation of the rock magnetization and the inhomogeneous distribution of the crustal physical properties. In fact, standard Poisson's analysis is based on homogeneity and uniformity criteria about the gravity and magnetic fields source distributions, which makes itself not suitable for multisource detection; moreover, when using RTP magnetic data the results are often limited due to the difficult access of information about the remanent magnetization.

These limitations are crucial when studying the seamounts geophysical properties, as inhomogeneities in terms of magnetization distribution are expected, mostly due to hydrothermal activity and resulting demagnetization (e.g., Caratori Tontini et al., 2010; Faggioni et al., 1995). In addition, the progressive evolution of the seamounts structure may result in a different orientation of the rocks magnetization associated with the change in the induced geomagnetic field (e.g., Cocchi et al., 2023).

Simulating the case of an inhomogeneous seamount is necessary to show the suitability of the method. To this end, we considered a seamount composed of three adjacent sectors with different magnetization intensity and orientation. The resulting magnetic map clearly showed the strong effect of source remanent magnetization. This case in fact is very similar to what observed above different seamounts in the aeromagnetic map of Southern

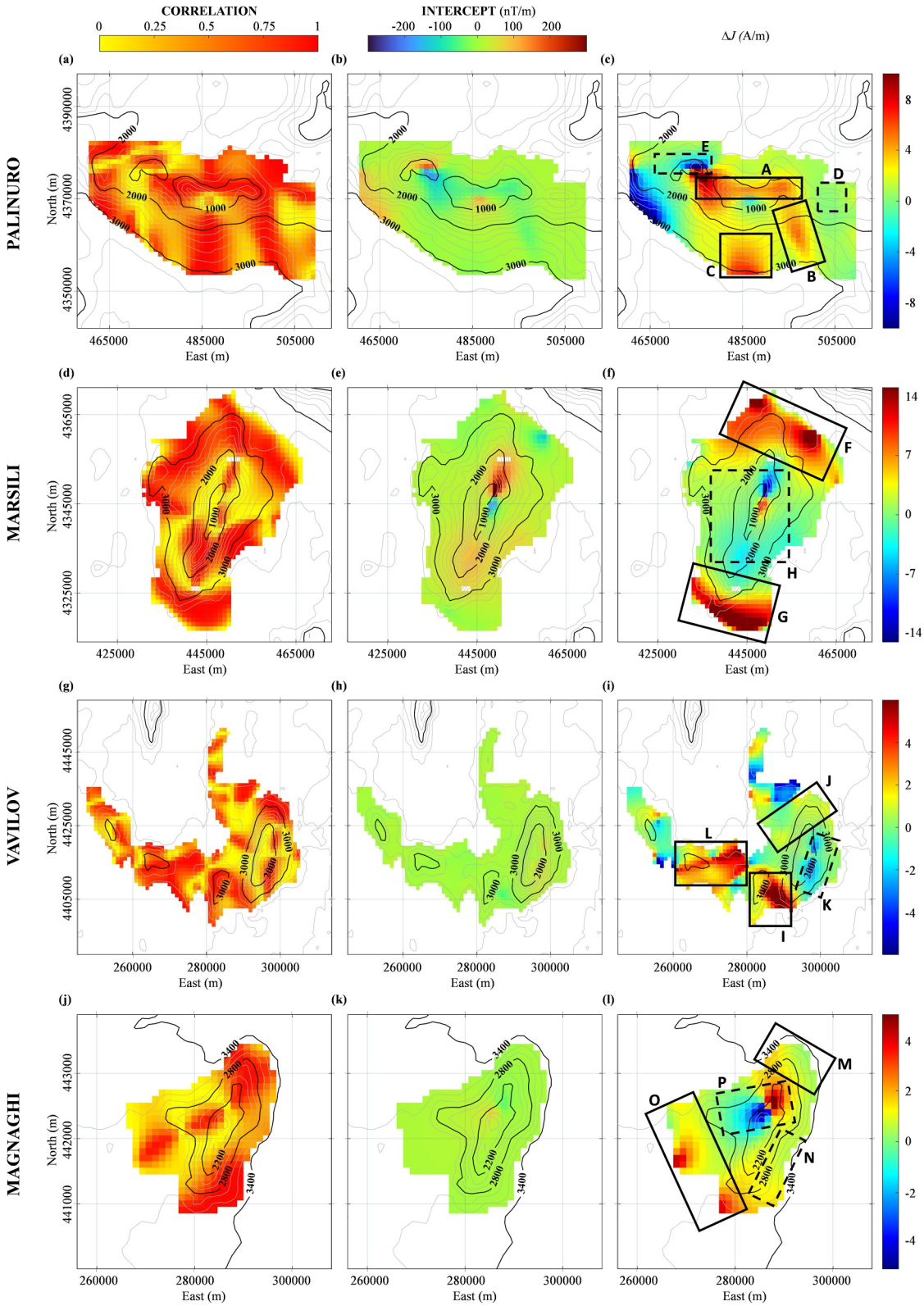

Figure 7. Results of the Poisson's analysis for Tyrrhenian seamounts. Maps of the (a, d, g, j) correlation, (b, e, h, k) intercept (K) coefficients and (c, f, i, l) the estimated ΔJ for the Palinuro, Marsili, Vavilov and Magnaghi seamounts, respectively. The black and gray contour lines represent the seamounts bathymetry. Solid squares indicate the main magnetized sectors of the seamounts; dashed squares are the areas of negative values and those of anomalies interference (see text).

Tyrrhenian Sea (e.g., Faggioni et al., 1995). We have verified the results of the analysis first computing the RTP anomalies using the correct inclination and declination of the magnetization. In this case, we were able to successfully identify the ΔJ with low uncertainty. We also note that more accurate results are inferred where the expected ΔJ was higher, that is, at the central area, with $\Delta J \sim 10$ A/m. The simulation also points out the limitation of the analysis with the RTP computation when there is no information available about the source remanent magnetization. Using instead the total gradients of potential fields we achieved a good identification of the inhomogeneous areas of the seamount.

Therefore, the proposed approach turns out to be the best choice to study the Tyrrhenian seamounts for several reasons:

1. A window-by-window analysis allows the inhomogeneity of seamounts to be inferred and it is appropriate to reduce the interference effects among anomalies (Chandler et al., 1981);
2. The approach based on the total gradients of the fields, Equation 4, ensures high resolution and a better discrimination of the single effects associated with adjacent sources
3. The performed Poisson's analysis is almost independent of the inclination and declination of the source magnetization, providing a more robust interpretation of anomalies having strong effects of remanent magnetization (e.g., Milano et al., 2019).

However, this analysis has also provided unsuitable areas for ΔJ estimation, mainly located nearby the transition zones with different ΔJ, which may reproduce the effect of rock demagnetization due to hydrothermal activities. Although these areas, characterized by negative MDR values, must be excluded for the evaluation of the physical properties of the source, they can nevertheless help to determine the region of inhomogeneous magnetization.

We found different densities for Palinuro and Marsili ($\rho \sim 2{,}100$ kg/m^3) and for Vavilov and Magnaghi ($\rho \sim 2{,}600$ kg/m^3) seamounts. These results are in good agreement with previous interpretation based on forward and inverse modeling of gravity data (e.g., Caratori Tontini et al., 2010; Fedi, 1997; Ligi et al., 2014). In particular, several studies dealt with the surprisingly low rocks density of the Marsili and Palinuro seamounts (e.g., Caratori Tontini et al., 2010; Innangi et al., 2016; Italiano et al., 2014; Ligi et al., 2014; Paltrinieri et al., 2022; Trua et al., 2002). The most reliable explanation lies in the intense hydrothermal circulation and subsequent alteration of the basalts (e.g., Caratori Tontini et al., 2010; Ligi et al., 2014; Lupton et al., 2008). The flow of hydrothermal fluids in seamount rocks, in fact, can produce physicochemical alterations followed by the formation of secondary hydrated phases (e.g., Woodward & Mumme, 1993) and new mineral groups that reach equilibrium through dissolution and precipitation processes (e.g., Pirajno, 2010). Moreover, hydrothermal alteration largely impacts the porosity and permeability of the rocks as well as its density/magnetization (e.g., Wyering et al., 2014).

For example, DTM-based morphometry study has shown areas of Palinuro with fine grained sediment infilling (Passaro et al., 2010); low density sediments have been observed also at Marsili (Del Monte et al., 1972), where dredged samples have revealed a high vesicularity reaching 30 vol. percentage (Trua et al., 2002). Submarine eruptions can, in fact, produce low density products as pillow lavas, sheet flows and hyaloclastites also reaching $\rho \sim 2{,}000$ kg/m^3 (Bonatti & Harrison, 1988; Schiffmann et al., 2006), and hydrothermal activity acts for a further decrease (Woodward & Mumme, 1993). Similar cases have also been found in other marine hydrothermal districts, such as at the Axial seamount off the Oregon coast, where porous features and hydrothermal vents have been observed on the seafloor, considered indicators of high subsurface permeability associated with low-density zones (Gilbert et al., 2007).

Similarities can also be found with studies conducted along the seamounts of the Bonin Arc (Western Pacific). Here, Ishihara (1987) discussed about the relationship between the seamount rock density and its average depth. According to the author, density increases rapidly at about 1 km depth, probably associated with a decrease in porosity. This observation seems to fit well with the densities we estimated and their relationship to seamount depth. Accordingly, we observe a good correspondence between the low rock densities, the high porosity and the shallow depth to the top of the Marsili and Palinuro seamounts (about 570 m b.s.l and 70 m b.s.l, respectively), while higher density values correspond well to the deeper Magnaghi and Vavilov seamounts (about 1,500 m b.s.l and 800 m b.s.l, respectively).

Poisson's analysis proved to be challenging compared to the problems already emerged from the synthetic case. Indeed, the agreement between total gradient magnetic and gravity anomalies is complicated due to: (a) the

interference from nearby sources (Palinuro seamount); (b) the magnetization distribution is much more complex than the density distribution (Marsili seamount, Vavilov seamount), as we may observe demagnetized areas or interferences with deep and/or lateral cone sources (Magnaghi seamount). For these reasons, we observed a good agreement between the volcanic bathymetry and the total gradient of the gravity field, while the magnetic anomalies are often shifted versus the volcanic edifices and present two or more highs.

In the case of Palinuro seamount, we have identified three areas with ΔJ up to 10 A/m. These are located at the central western ("A" in Figure 7c), central eastern ("B" in Figure 7c) and southern ("C" in Figure 7c) subportions of the seamount which, according to Colantoni et al. (1981), represent the regions with highest magnetization. The areas "B" and "C" are also compatible with the presence of magnetic morphological and dike-like structures, as argued by Caratori Tontini et al. (2009). On the contrary, the observed alternation of negative, positive and vanishing ΔJ values at the western sector ("E" in Figure 7c) is probably related to strong inhomogeneities and demagnetization phenomena; this is supported by previous studies which interpreted the western area of this seamount as being strongly influenced by hydrothermal activity (e.g., Caratori Tontini et al., 2009; Caratori Tontini et al., 2014; Cocchi et al., 2021; Colantoni et al., 1981; Ligi et al., 2014). We also observe $\Delta J \sim 0$ at the eastern crest of Palinuro ("D" in Figure 7c), in agreement with the hypothesis of nonmagnetic sediments (Caratori Tontini et al., 2009). Our estimated values are compatible with the $J \sim 5$ and 8 A/m obtained by Cocchi et al. (2021) and Caratori Tontini et al. (2009), respectively, from the inverse and forward modeling of magnetic data.

For the Marsili seamount, we have clearly identified a central portion ("H" in Figure 7f) characterized by the alternation of negative, positive and very low ΔJ values, suggesting rocks inhomogeneities; indeed, this sector is characterized by a strong hydrothermal activities leading to both collapses and strong demagnetization (e.g., Caratori Tontini et al., 2010; Caratori Tontini et al., 2014; Faggioni et al., 1995); moreover, several studies indicated also the presence of a shallow and active nonmagnetic magma chamber below this area (e.g., Caratori Tontini et al., 2010; Caratori Tontini et al., 2014; Trua et al., 2002); it follows that in this portion of the seamount it is not possible to determine the effective rock magnetization. Nevertheless, we note that the resulting magnetization distribution is within the ∼3–20 A/m range estimated from the analysis of rock samples (Table 1 in Faggioni et al., 1995). In particular, we identified two strongly magnetized areas to the southern ("G" in Figure 7f) and northern ("F" in Figure 7f) ends of the volcanic edifice, in agreement with results obtained from 3D inverse modeling of magnetic data by Cocchi et al. (2009), who considered these zones as those with the highest values of rock magnetization.

The Vavilov seamount has certainly represented the most complicated case study; indeed, several strong inhomogeneities and the presence of reversely magnetized rocks are expected, which resulted in a strong magnetic anomaly with reversed dipolarity with respect to the present geomagnetic field orientation. In general, the spreading of the volcanic edifice occurred during different magnetic epochs where deep and shallow bodies with different magnetic features produces fields overlapping each other (e.g., Cocchi et al., 2023). Possible past hydrothermal activities were hypothesized (e.g., Bertand et al., 1990; Caratori Tontini et al., 2010; Faggioni et al., 1995) as well a collapse of its western flank (e.g., Cocchi et al., 2023). These phenomena may affect the results of the Poisson's analysis leading to alternation of negative ("K" in Figure 7i), positive and vanishing ΔJ values. We estimated $\Delta J \sim 2$ A/m along the main volcanic edifice ("J" in Figure 7i) and $\Delta J \sim 7$ A/m in the surrounding basin ("I," "L" in Figure 7i), which are again consistent with previous interpretations (Faggioni et al., 1995).

Finally, in the last case (the Magnaghi seamount) we have identified two subportions as most magnetized regions, with estimated ΔJ that can reach 5 A/m ("M," "O" in Figure 7l). In the southern part ("N" in Figure 7l), we instead estimated lower values of about ∼2 A/m, in agreement with Faggioni et al. (1995) and Fedi et al. (1994), who identified rock magnetization from 1 to 2 A/m in the southern slope of the seamount; the presence of negative values at its central subpart ("P" in Figure 7l) confirmed the detected rocks inhomogeneities. Table 1 summarizes the comparison of our results and the previously published values of rock magnetization.

6. Conclusions

Our approach based on the Poisson's analysis of potential field data represents a successful strategy to map geological structures trough the non-invasive and low-cost geophysical techniques, which can be particularly suitable in areas of difficult access. In particular, the study of the total gradient anomalies proved to be an effective approach to overcome the problems of the strong remanent magnetization and to reduce the effect of anomalies interference.

Table 1
Summary of the Magnetization Values for Southern Tyrrhenian Seamounts From This Study and Other Works

	This study (A/m)	Other studies[a] (A/m)
PALINURO	8–10 (A: Northern sector)	8 (Caratori Tontini et al., 2009)
	6–8 (B–C: Southern sector)	5 (Cocchi et al., 2021)
MARSILI	7–15 (F: Northern sector)	3–20 (Faggioni et al., 1995)
	5–>15 (G: Southern sector)	6–11 (Cocchi et al., 2009)
VAVILOV	~2 (J: Northern sector)	1.5–2.5 (Faggioni et al., 1995)
	~7 (I–L: Vavilov basin)	1–8.5 (Vavilov basin, Faggioni et al., 1995)
MAGNAGHI	~2 (M: Northern sector)	2.3–4.9 (Faggioni et al., 1995)
	~2 (N: Eastern sector)	<2 (Fedi et al., 1994)
	~5 (O: Southwestern sector)	

Note. Capital letters indicate seamounts sectors highlighted in Figure 7. [a]Values are referred to the entire volcanic edifice.

The test of the Poisson's window-based analysis and on the total gradients of potential fields allowed a good identification of the three inhomogeneous areas of the model with a reduced ΔJ uncertainty. However, we showed that the method may fail nearby the transitions of ΔJ. At the same time this limitation can be used for individuating areas of rocks demagnetization because of hydrothermal activities since in these areas we expect sudden ΔJ changes. In the real case, the total gradient maps show an unclear correspondence between magnetic and gravity anomalies due to interference from nearby sources (Palinuro seamount), complex magnetization distribution versus uniform density distribution (Marsili seamount, Vavilov seamount) including demagnetized areas, and possible deep interfering magnetic sources lateral to the cone (Magnaghi seamount). Thus, while the total gradient of the gravity field mainly reflects the volcanic bathymetry, the total gradient of the magnetic field is characterized by two or more highs, not centered on the volcanic edifices. Nevertheless, based on the criteria established from the synthetic tests, we were able to provide ΔJ estimates in local subregions of the seamounts.

We may conclude that, despite the complexity of the geological structures, a window-by-window correlation analysis allows inferring the main seamounts rocks properties. The best advantage of this technique is that it does not require a-priori information and involves low computational costs. In the case of the main seamounts of the Southern Tyrrhenian Sea, our analysis provides useful insights on the inhomogeous magnetization of the seamounts, also associated with hydrothermal activity, which can be used as a starting information for further inverse and forward modeling of potential field data.

Data Availability Statement

The total gradient data sets used for the correlation analysis of the Tyrrhenian seamounts are available at Barone et al. (2024). The gravity and magnetic unprocessed data sets were digitalized from the raster maps available at the ISPRA website: http://portalesgi.isprambiente.it/index.php/en/elenco-base-dati/15.

Acknowledgments
The authors would like to express their sincere gratitude to one anonymous Reviewer and Dr. Andrea Vitale whose comments contributed to highly improve our manuscript. Open access publishing facilitated by Universita degli Studi di Napoli Federico II, as part of the Wiley - CRUI-CARE agreement.

References

AGIP. (1981). *Carta aeromagnetica d'Italia (scala 1:500.000)*. Attività Mineraria Direzione Esplorazione. Donato Milanese.

Alencar de Matos, C., & Mendonça, C. A. (2020). Poisson magnetization-to-density-ratio and magnetization inclination properties of banded iron formations of the Carajás mineral province from processing airborne gravity and magnetic data. *Geophysics*, *85*(5), K1–K11. https://doi.org/10.1190/geo2019-0421.1

Barbosa, V. C., & Silva, J. B. (2011). Reconstruction of geologic bodies in depth associated with a sedimentary basin using gravity and magnetic data. *Geophysical Prospecting*, *59*(6), 1021–1034. Advances in Electromagnetic, Gravity and Magnetic Methods for Exploration. https://doi.org/10.1111/j.1365-2478.2011.00997.x

Barone, A., Milano, M., & Fedi, M. (2024). Inhomogeneous magnetization of Tyrrhenian seamounts revealed from gravity and magnetic correlation analysis [Dataset]. *Zenodo*. https://doi.org/10.5281/zenodo.12799438

Beccaluva, L., Bonatti, E., Dupuy, C., Ferrara, G., Innocenti, F., Lucchini, F., et al. (1990). Geochemistry and mineralogy of volcanic rocks from ODP sites 650, 651, 655 and 654 in the Tyrrhenian Sea. In *Proceedings of the ocean drilling program, scientific results* (Vol. 107, pp. 49–74). Ocean Drilling Program. https://doi.org/10.2973/odp.proc.sr.107.140.1990

Bertrand, H., Boivin, P., & Robin, C. (1990). Petrology and geochemistry of basalts from the Vavilov basin (Tyrrhenian sea), Ocean drilling program Leg 107, Holes 651A and 655B. In *Proceedings of the ocean drilling program. Scientific results* (Vol. 107, pp. 75–92). US Gov. Print. Off.

Blakely, R. J. (1996). *Potential theory in gravity and magnetic applications*. Cambridge University Press. Retrieved from https://market.android.com/details?id=book-qGZV-P8bt6gC

Bonatti, E., & Harrison, C. G. A. (1988). Eruption styles of basalt in oceanic spreading ridges and seamounts: Effect of magma temperature and viscosity. *Journal of Geophysical Research*, *93*, B4–B2980. https://doi.org/10.1029/JB093iB04p02967

Bonatti, E., Honnorez, J., Joensuu, O., Rydell, H. S., & Beyth, M. (1972). Submarine iron deposits from the mediterranean sea. In D. J. Stanley (Ed.), *The Mediterranean sea* (pp. 701–710). Hutchinson and Ross.

Caratori Tontini, F., Bortoluzzi, G., Carmisciano, C., Cocchi, L., De Ronde, C. E. J., Ligi, M., & Muccini, F. (2014). Near-bottom magnetic signatures of submarine hydrothermal systems at Marsili and Palinuro volcanoes, southern Tyrrhenian Sea, Italy. *Economic Geology*, *109*(8), 2119–2128. https://doi.org/10.2113/econgeo.109.8.2119

Caratori Tontini, F., Cocchi, L., & Carmisciano, C. (2009). Rapid 3-D forward model of potential fields with application to the Palinuro Seamount magnetic anomaly (southern Tyrrhenian Sea, Italy). *Journal of Geophysical Research*, *114*(B2). https://doi.org/10.1029/2008jb005907

Caratori Tontini, F., Cocchi, L., Muccini, F., Carmisciano, C., Marani, M., Bonatti, E., et al. (2010). Potential-field modeling of collapse-prone submarine volcanoes in the southern Tyrrhenian Sea (Italy). *Geophysical Research Letters*, *37*(3). https://doi.org/10.1029/2009gl041757

Caratori Tontini, F., Stefanelli, P., Giori, I., Faggioni, O., & Carmisciano, C. (2004). The revised aeromagnetic anomaly map of Italy. *Annals of Geophysics*, *47*, 1547–1555.

Carminati, E., Wortel, M. J. R., Spakman, W., & Sabadini, R. (1998). The role of slab detachment processes in the opening of the western–central Mediterranean basins: Some geological and geophysical evidence. *Earth and Planetary Science Letters*, *160*(3), 651–665. https://doi.org/10.1016/S0012-821X(98)00118-6

Carrozzo, M. T., Chirenti, A., Luzio, D., Margiotta, C., Quarta, T., & Zuani, F. (1981). Carta Gravimetrica d'Italia: Tecniche automatiche per la sua realizzazione. *Atti del I Convegno GNGTS*.

Carrozzo, M. T. (1981). Carta Gravimetrica d'Italia: Tecniche automatiche per la sua realizzazione. *Atti del I Convegno GNGTS*.

Cassano, E., Fichera, R., & Arisi Rota, F. (1986a). Rilievo Aeromagnetico D'italia: Alcuni Risultati Interpretativi. In *Atti del v Convegno Annuale del Gruppo Nazionale di Geofisica della Terra Solida; CNR: Roma, Italy* (Vol. 2, pp. 939–962).

Cassano, E., Fichera, R., & Arisi Rota, F. (1986b). *Rilievo aeromagnetico d'Italia. Alcuni risultati interpretativi* (pp. 939–958). Atti del V Convegno GNGTS.

Cavinato, G. P., & Celles, P. D. (1999). Extensional basins in the tectonically bimodal central Apennines fold-thrust belt, Italy: Response to corner flow above a subducting slab in retrograde motion. *Geology*, *27*(10), 955–958. https://doi.org/10.1130/0091-7613(1999)027<0955:ebittb>2.3.co;2

Cella, F., Fedi, M., Florio, G., Paoletti, V., & Rapolla, A. (2008). A review of the gravity and magnetic studies in the Tyrrhenian Basin and its volcanic districts. *Annals of Geophysics*, *60*(6 Sup), GM674. https://doi.org/10.4401/ag-7550

Cella, F., Fedi, M., Florio, G., & Rapolla, A. (1998). Boundaries of magnetic anomaly sources in the Tyrrhenian region. *Annals of Geophysics*, *41*(3). https://doi.org/10.4401/ag-4349

Chandler, V. W., Koski, J. S., Hinze, W. J., & Braile, L. W. (1981). Analysis of multisource gravity and magnetic anomaly data sets by moving-window application of Poisson's theorem. *Geophysics*, *46*(1), 30–39. https://doi.org/10.1190/1.1441136

Chandler, V. W., & Malek, K. C. (1991). Moving-window Poisson analysis of gravity and magnetic data from the Penokean orogen, east-central Minnesota. *Geophysics*, *56*(1), 123–132. https://doi.org/10.1190/1.1442948

Chiappini, M., Meloni, A., Boschi, E., Faggioni, O., Beverini, N., Carmisciano, C., & Marson, I. (2000). Shaded relief magnetic anomaly map of Italy and surrounding marine areas. *Annals of Geophysics*, *43*(5). https://doi.org/10.4401/ag-3676

Chiarabba, C., De Gori, P., & Speranza, F. (2008). The southern Tyrrhenian subduction zone: Deep geometry, magmatism and Plio-Pleistocene evolution. *Earth and Planetary Science Letters*, *268*(3), 408–423. https://doi.org/10.1016/j.epsl.2008.01.036

Cocchi, L., Caratori Tontini, F., Carmisciano, C., & Marani, M. (2008). Tortonian-pleistocenic oceanic features in the southern Tyrrhenian Sea: Magnetic inverse model of the Selli-Vavilov region. *Marine Geophysical Researches*, *29*(4), 251–266. https://doi.org/10.1007/s11001-009-9061-5

Cocchi, L., Caratori Tontini, F., Muccini, F., & de Ronde, C. E. J. (2021). Magnetic expression of hydrothermal systems hosted by submarine calderas in subduction settings: Examples from the Palinuro and Brothers volcanoes. *Geosciences Journal*, *11*(12), 504. https://doi.org/10.3390/geosciences11120504

Cocchi, L., Caratori Tontini, F., Muccini, F., Marani, M. P., Bortoluzzi, G., & Carmisciano, C. (2009). Chronology of the transition from a spreading ridge to an accretional seamount in the Marsili backarc basin (Tyrrhenian Sea). *Terra Nova*, *21*, 5–374. https://doi.org/10.1111/j.1365-3121.2009.00891.x

Cocchi, L., Muccini, F., Palmiotto, C., & Ventura, G. (2023). Imaging the plumbing system of the asymmetric Vavilov spreading ridge (Tyrrhenian Sea back-arc basin) from combined bathymetry and magnetic data. *Geophysical Research Letters*, *50*(22), e2023GL105196. https://doi.org/10.1029/2023gl105196

Colantoni, P., Lucchini, F., Rossi, P. L., Sartori, R., & Savelli, C. (1981). The Palinuro volcano and magmatism of the southeastern Tyrrhenian Sea (Mediterranean). *Marine Geology*, *39*(1–2), M1–M12. https://doi.org/10.1016/0025-3227(81)90020-7

Contrucci, I., Mauffret, A., Brunet, C., Nercessian, A., Béthoux, N., & Ferrandini, J. (2005). Deep structure of the North Tyrrhenian Sea from multi-channel seismic profiles and on land wide angle reflection/refraction seismic recording (LISA cruise): Geodynamical implications. *Tectonophysics*, *406*(3–4), 141–163. https://doi.org/10.1016/j.tecto.2005.05.015

Contrucci, I., Nercessian, A., Béthoux, N., Mauffret, A., & Pascal, G. (2001). A Ligurian (western Mediterranean Sea) geophysical transect revisited. *Geophysical Journal International*, *146*(1), 74–97. https://doi.org/10.1046/j.0956-540x.2001.01418.x

Cordell, L., & Taylor, P. T. (1971). Investigation of magnetization and density of a North Atlantic seamount using Poisson's theorem. *Geophysics*, *36*(5), 919–937. https://doi.org/10.1190/1.1440224

Dekov, V. M., Kamenov, G. D., Savelli, C., Stummeyer, J., Thiry, M., Shanks, W., et al. (2009). Metalliferous sediments from Eolo Seamount (Tyrrhenian Sea): Hydrothermal deposition and re-deposition in a zone of oxygen depletion. *Chemical Geology*, *264*(1–4), 347–363. https://doi.org/10.1016/j.chemgeo.2009.03.023

Dekov, V. M., & Savelli, C. (2004). Hydrothermal activity in the SE Tyrrhenian Sea: An overview of 30 years of research. *Marine Geology*, *204*(1–2), 161–185. https://doi.org/10.1016/s0025-3227(03)00355-4

Del Ben, A., Barnaba, C., & Taboga, A. (2008). Strike-slip systems as the main tectonic features in the Plio-Quaternary kinematics of the Calabrian Arc. *Marine Geophysical Researches*, *29*, 1–12. https://doi.org/10.1007/s11001-007-9041-6

Del Monte, M. (1972). Il vulcanesimo del Mar Tirreno-nota preliminare sui vulcani Marsili e Palinuro. *Giornale di Geologia*, *38*, 231–252.

De Ritis, R., Ventura, G., Chiappini, M., Carluccio, R., & von Frese, R. (2010). Regional magnetic and gravity anomaly correlations of the Southern Tyrrhenian Sea. *Physics of the Earth and Planetary Interiors*, *181*(1), 27–41. https://doi.org/10.1016/j.pepi.2010.04.003

Doglioni, C., Innocenti, F., Morellato, C., Procaccianti, D., & Scrocca, D. (2004). On the Tyrrhenian Sea opening. *Memorie Descrittive della Carta Geologica d'Italia*, *44*, 147–164.
Doglioni, C., Mongelli, F., & Pieri, P. (1994). The Puglia uplift (SE Italy): An anomaly in the foreland of the Apenninic subduction due to buckling of a thick continental lithosphere. *Tectonics*, *13*(5), 1309–1321. https://doi.org/10.1029/94tc01501
Doo, W.-B., Hsu, S.-K., Tsai, C.-H., & Huang, Y.-S. (2009). Using analytic signal to determine magnetization/density ratios of geological structures. *Geophysical Journal International*, *179*(1), 112–124. https://doi.org/10.1111/j.1365-246X.2009.04297.x
Faccenna, C., Becker, T. W., Lucente, F. P., Jolivet, L., & Rossetti, F. (2001). History of subduction and back arc extension in the Central Mediterranean. *Geophysical Journal International*, *145*(3), 809–820. https://doi.org/10.1046/j.0956-540x.2001.01435.x
Faccenna, C., Jolivet, L., Piromallo, C., & Morelli, A. (2003). Subduction and the depth of convection in the Mediterranean mantle. *Journal of Geophysical Research*, *108*(B2). https://doi.org/10.1029/2001JB001690
Faccenna, C., Mattei, M., Funiciello, R., & Jolivet, L. (1997). Styles of back-arc extension in the central Mediterranean. *Terra Nova*, *9*(3), 126–130. https://doi.org/10.1046/j.1365-3121.1997.d01-12.x
Faggioni, O., Pinna, E., Savelli, C., & Schreider, A. A. (1995). Geomagnetism and age study of Tyrrhenian seamounts. *Geophysical Journal International*, *123*(3), 915–930. https://doi.org/10.1111/j.1365-246X.1995.tb06898.x
Fedi, M. (1997). Estimation of density, magnetization, and depth to source: A nonlinear and noniterative 3-D potential-field method. *Geophysics*, *62*(3), 814–830. https://doi.org/10.1190/1.1444191
Fedi, M., Florio, G., & Rapolla, A. (1994). The Magnaghi seamount: A gravimetric and magnetic combined study. *Bollettino di Geofisica Teorica ed Applicata*, *36*(141–144), 523–531.
I. R. Finetti (Ed.) (2005)., *CROP project: Deep seismic exploration of the central Mediterranean and Italy*. Elsevier.
Florio, G., Fedi, M., & Cella, F. (2011). Insights on the spreading of the Tyrrhenian Sea from the magnetic anomaly pattern: Magnetic anomaly pattern in the Tyrrhenian Sea. *Terra Nova*, *23*(2), 127–133. https://doi.org/10.1111/j.1365-3121.2011.00992.x
Florio, G., Milano, M., & Cella, F. (2021). Gravity mapping of basement depth in seismogenic, fault-controlled basins: The case of Middle Aterno Valley (Central Italy). *Tectonophysics*, *817*, 229044. https://doi.org/10.1016/j.tecto.2021.229044
Florio, G., Passaro, S., de Alteriis, G., & Cella, F. (2022). Magnetic anomalies of the Tyrrhenian Sea revisited: A processing workflow for enhancing the resolution of aeromagnetic data. *Geosciences Journal*, *12*(10), 377. https://doi.org/10.3390/geosciences12100377
Gamberi, F., Marani, M., & Savelli, C. (1997). Tectonic, volcanic and hydro-thermal features of a submarine portion of the Aeolian arc (Tyrrhenian Sea). *Marine Geology*, *140*(1–2), 167–181. https://doi.org/10.1016/s0025-3227(97)00020-0
Gantar, C., Morelli, C., & Pisani, M. (1968). Information report on surface gravity and magnetic measurements with the Ship" Bannock. In *The Mediterranean sea* (pp. 1965–1968.5). Consiglio nazionale delle ricerche.
Garland, G. D. (1951). Combined analysis of gravity and magnetic anomalies. *Geophysics*, *16*(1), 51–62. https://doi.org/10.1190/1.1437650
Gilbert, L. A., McDuff, R. E., & Paul Johnson, H. (2007). Porosity of the upper edifice of axial seamount. *Geology*, *35*(1), 49–52. https://doi.org/10.1130/g22892a.1
Gvirtzman, Z., & Nur, A. (2001). Residual topography, lithospheric structure and sunken slabs in the central Mediterranean. *Earth and Planetary Science Letters*, *187*(1–2), 117–130. https://doi.org/10.1016/s0012-821x(01)00272-2
Hinze, W. J., Von Frese, R. R., Von Frese, R., & Saad, A. H. (2013). *Gravity and magnetic exploration: Principles, practices, and applications*. Cambridge University Press.
Innangi, S., Passaro, S., Tonielli, R., Milano, G., Ventura, G., & Tamburrino, S. (2016). Seafloor mapping using high-resolution multibeam backscatter: The Palinuro seamount (eastern Tyrrhenian Sea). *Journal of Maps*, *12*(5), 736–746. https://doi.org/10.1080/17445647.2015.1071719
Ishihara, T. (1987). Gravimetric determination of densities of seamounts along the Bonin Arc. *Seamounts, Islands, And Atolls*, *43*, 97–113. https://doi.org/10.1029/gm043p0097
ISPRA, ENI, OGS. (2009). Cartografia Gravimetrica Digitale d'Italia alla scala 1:250.000. [Dataset]. https://www.isprambiente.gov.it/it/progetti/cartella-progetti-in-corso/suolo-e-territorio-1/cartografia-gravimetrica-digitale
Italiano, F., De Santis, A., Favali, P., Rainone, M. L., Rusi, S., & Signanini, P. (2014). The Marsili volcanic seamount (southern Tyrrhenian Sea): A potential offshore geothermal resource. *Energies*, *7*(7), 4068–4086. https://doi.org/10.3390/en7074068
Kanasewich, E. R., & Agarwal, R. G. (1970). Analysis of combined gravity and magnetic fields in wave number domain. *Journal of Geophysical Research*, *75*(29), 5702–5712. https://doi.org/10.1029/jb075i029p05702
Kastens, K., Mascle, J., Auroux, C., Bonatti, E., Broglia, C., Channell, J., et al. (1988). ODP Leg 107 in the Tyrrhenian Sea: Insights into passive margin and back-arc basin evolution. *Geological Society of America Bulletin*, *100*(7), 1140–1156. https://doi.org/10.1130/0016-7606(1988)100<1140:olitts>2.3.co;2
Kelemework, Y., Milano, M., La Manna, M., de Alteriis, G., Iorio, M., & Fedi, M. (2021). Crustal structure in the Campanian region (Southern Apennines, Italy) from potential field modelling. *Scientific Reports*, *11*(1), 14510. https://doi.org/10.1038/s41598-021-93945-8
Ligi, M., Cocchi, L., Bortoluzzi, G., D'Oriano, F., Muccini, F., Tontini, F. C., et al. (2014). Mapping of seafloor hydrothermally altered rocks using geophysical methods: Marsili and Palinuro seamounts, southern Tyrrhenian Sea. *Economic Geology and the Bulletin of the Society of Economic Geologists*, *109*(8), 2103–2117. https://doi.org/10.2113/econgeo.109.8.2103
Liu, S., Fedi, M., Hu, X., Baniamerian, J., Wei, B., Zhang, D., & Zhu, R. (2018). Extracting induced and remanent magnetizations from magnetic data modeling. *Journal of Geophysical Research: Solid Earth*, *123*(11), 9290–9309. https://doi.org/10.1029/2017JB015364
Loreto, M. F., Düşünür-Doğan, D., Üner, S., İşcan-Alp, Y., Ocakoğlu, N., Cocchi, L., et al. (2019). Fault-controlled deep hydrothermal flow in a back-arc tectonic setting, SE Tyrrhenian Sea. *Scientific Reports*, *9*(1), 17724. https://doi.org/10.1038/s41598-019-53696-z
Lupton, J., De Ronde, C., Beker, E., Italiano, F., Sprovieri, M., Bruno, P. P., …, & Walker, S. (2008). Submarine hydrothermal activity on the Aeolian arc: New evidence from helium isotopes. In *AGU fall meeting*. American Geophysical Union.
Malinverno, A., & Ryan, W. B. (1986). Extension in the Tyrrhenian Sea and shortening in the Apennines as result of arc migration driven by sinking of the lithosphere. *Tectonics*, *5*(2), 227–245. https://doi.org/10.1029/tc005i002p00227
Mancini, M., & Cavinato, G. P. (2009). The Middle Valley of the Tiber River, central Italy: Plio-Pleistocene fluvial and coastal sedimentation, extensional tectonics and volcanism. In *Fluvial Sedimentology VII* (pp. 373–396). Blackwell Publishing Ltd. https://doi.org/10.1002/9781444304350.ch20
Marani, M. P., & Trua, T. (2002). Thermal constriction and slab tearing at the origin of a superinflated spreading ridge: Marsili volcano (Tyrrhenian Sea). *Journal of Geophysical Research*, *107*(B9), EPM–3. https://doi.org/10.1029/2001jb000285
Mendonça, C. A. (2004). Automatic determination of the magnetization–density ratio and magnetization inclination from the joint interpretation of 2D gravity and magnetic anomalies. *Geophysics*, *69*(4), 938–948. https://doi.org/10.1190/1.1778237
Milano, G., Passaro, S., & Sprovieri, M. (2012). Present-day knowledge on the Palinuro seamount (south-eastern Tyrrhenian Sea). *Bollettino di Geofisica Teorica ed Applicata*, *53*(4).

Milano, M., Fedi, M., & Fairhead, J. D. (2019). Joint analysis of the magnetic field and total gradient intensity in central Europe. *Solid Earth Discussions*, 1–26. https://doi.org/10.5194/se-2019-40

Milano, M., Kelemework, Y., La Manna, M., Fedi, M., Montanari, D., & Iorio, M. (2020). Crustal structure of Sicily from modelling of gravity and magnetic anomalies. *Scientific Reports*, *10*(1), 16019. https://doi.org/10.1038/s41598-020-72849-z

Milano, M., Varfinezhad, R., Bizhani, H., Moghadasi, M., Kalateh, A. N., & Baghzendani, H. (2021). Joint interpretation of magnetic and gravity data at the Golgohar mine in Iran. *Journal of Applied Geophysics*, *195*, 104476. https://doi.org/10.1016/j.jappgeo.2021.104476

Milia, A., Turco, E., Pierantoni, P. P., & Schettino, A. (2009). Four-dimensional tectono-stratigraphic evolution of the southeastern peri-Tyrrhenian basins (margin of Calabria, Italy). *Tectonophysics*, *476*(1–2), 41–56. https://doi.org/10.1016/j.tecto.2009.02.030

Minniti, M., & Bonavia, F. F. (1984). Copper-ore grade hydrothermal mineralization discovered in a seamount in the Tyrrhenian Sea (Mediterranean): Is the mineralization related to porphyry-coppers or to base metal lodes? *Marine Geology*, *59*(1–4), 271–282. https://doi.org/10.1016/0025-3227(84)90097-5

Morelli, C., Gantar, C., & Pisani, M. (1975). Bathymetry, gravity and magnetism in the strait of Sicily and in the Ionian sea. *Boll. Geof. Teor. Appl.*, *17*, 39–58.

Morelli, C., Pisani, M., & Gantar, C. (1975). Geophysical studies in the Aegean Sea and in the eastern Mediterranean. *Boll. Geof. Teor. Appl.*, *18*, 127–168.

Nabighian, M. N. (1972). The analytic signal of two-dimensional magnetic bodies with polygonal cross-section: Its properties and use for automated anomaly interpretation. *Geophysics*, *37*(3), 507–517. https://doi.org/10.1190/1.1440276

Nettleton, L. L. (1939). Determination of density for reduction of gravimeter observations. *Geophysics*, *4*(3), 176–183. https://doi.org/10.1190/1.0403176

Olesen, O., Brönner, M., Ebbing, J., Gellein, J., Gernigon, L., Koziel, J., et al. (2010). New aeromagnetic and gravity compilations from Norway and adjacent areas: Methods and applications. In *Geological Society, London, Petroleum Geology Conference Series, Geological Society, London, Petroleum Geology Conference Series* (Vol. 7, No. (1), pp. 559–586). https://doi.org/10.1144/0070559: The Geological Society of London.

Paltrinieri, D., Favali, P., Italiano, F., Signanini, P., Caso, C., & Armani, F. B. (2022). The Marsili seamount offshore geothermal reservoir: A big challenge for an energy transition model. *Energies*, *15*(5), 1900. https://doi.org/10.3390/en15051900

Panza, G. F., Peccerillo, A., Aoudia, A., & Farina, B. (2007). Geophysical and petrological modelling of the structure and composition of the crust and upper mantle in complex geodynamic settings: The Tyrrhenian Sea and surroundings. *Earth-Science Reviews*, *80*(1–2), 1–46. https://doi.org/10.1016/j.earscirev.2006.08.004

Parker, R. L. (1972). The rapid calculation of potential anomalies. *Geophysical Journal International*, *31*(4), 447–455. https://doi.org/10.1111/j.1365-246X.1973.tb06513.x

Passaro, S., Milano, G., D'Isanto, C., Ruggieri, S., Tonielli, R., Bruno, P. P., et al. (2010). DTM-based morphometry of the Palinuro seamount (Eastern Tyrrhenian Sea): Geomorphological and volcanological implications. *Geomorphology*, *115*(1–2), 129–140. https://doi.org/10.1016/j.geomorph.2009.09.041

Patacca, E., Sartori, R., & Scandone, P. (1990). Tyrrhenian basin and Apenninic arcs: Kinematic relations since late Tortonian times. *Memorie della Societa Geologica Italiana*, *45*, 425–451.

Patacca, E., & Scandone, P. (2001). Late thrust propagation and sedimentary response in the thrust-belt—Foredeep system of the Southern Apennines (Pliocene-Pleistocene). In G. B. Vai & I. P. Martini (Eds.), *Anatomy of an orogen: The Apennines and adjacent Mediterranean basins* (pp. 401–440). Springer Netherlands. https://doi.org/10.1007/978-94-015-9829-3_23

Pirajno, F. (2010). Intracontinental strike-slip faults, associated magmatism, mineral systems and mantle dynamics: Examples from NW China and Altay-Sayan (Siberia). *Journal of Geodynamics*, *50*(Issues 3–4), 325–346. https://doi.org/10.1016/j.jog.2010.01.018

Prada, M., Sallarès, V., Ranero, C. R., Vendrell, M. G., Grevemeyer, I., Zitellini, N., & de Franco, R. (2014). Seismic structure of the Central Tyrrhenian basin: Geophysical constraints on the nature of the main crustal domains. *Journal of Geophysical Research: Solid Earth*, *119*(1), 52–70. https://doi.org/10.1002/2013jb010527

Robin, C., Colantoni, P., Gennesseaux, M., & Rehault, J. P. (1987). Vavilov seamount: A mildly alkaline Quaternary volcano in the Tyrrhenian basin. *Marine Geology*, *78*(1–2), 125–136. https://doi.org/10.1016/0025-3227(87)90071-5

Roest, W. R., Verhoef, J., & Pilkington, M. (1992). Magnetic interpretation using the 3·D analytic signal. *Geophysics*, *57*(1), 116–125. https://doi.org/10.1190/1.1443174

Ross, H. P., & Lavin, P. M. (1966). In-situ determination of the remanent magnetic vector of two-dimensional tabular bodies. *Geophysics*, *31*(5), 949–962. https://doi.org/10.1190/1.1439826

Royden, L. H. (1988). Late Cenozoic tectonics of the Pannonian basin system: Chapter 3.

Sandwell, D. T., & Smith, W. H. F. (1997). Marine gravity anomaly from Geosat and ERS 1 satellite altimetry. *Journal of Geophysical Research*, *102*(B5), 10039–10054. https://doi.org/10.1029/96JB03223

Sartori, R., Torelli, L., Zitellini, N., Carrara, G., Magaldi, M., & Mussoni, P. (2004). Crustal features along a W–E Tyrrhenian transect from Sardinia to Campania margins (Central Mediterranean). *Tectonophysics*, *383*(3–4), 171–192. https://doi.org/10.1016/j.tecto.2004.02.008

Savelli, C. (1988). Late Oligocene to Recent episodes of magmatism in and around the Tyrrhenian Sea: Implications for the processes of opening in a young inter-arc basin of intra-orogenic (Mediterranean) type. *Tectonophysics*, *146*(1–4), 163–181. https://doi.org/10.1016/0040-1951(88)90089-3

Savelli, C. (2002). Time–space distribution of magmatic activity in the western Mediterranean and peripheral orogens during the past 30 Ma (a stimulus to geodynamic considerations). *Journal of Geodynamics*, *34*(1), 99–126. https://doi.org/10.1016/s0264-3707(02)00026-1

Savelli, C., & Ligi, M. (2017). An updated reconstruction of basaltic crust emplacement in Tyrrhenian Sea, Italy. *Scientific Reports*, *7*(1), 18024. https://doi.org/10.1038/s41598-017-17625-2

Savelli, C., & Schreider, A. A. (1991). The opening processes in the deep Tyrrhenian basins of Marsili and Vavilov, as deduced from magnetic and chronological evidence of their igneous crust. *Tectonophysics*, *190*(1), 119–131. https://doi.org/10.1016/0040-1951(91)90358-y

Schiffman, P., Watters, R. J., Thompson, N., & Walton, A. W. (2006). Hyaloclastites and the slope stability of Hawaiian volcanoes: Insights from the Hawaiian Scientific Drilling Project's 3-km drill core. *Journal of Volcanology and Geothermal Research*, *151*(1–3), 217–228. https://doi.org/10.1016/j.jvolgeores.2005.07.030

Schreider, A. A. (1993). Chronology of the oceanic linear magnetic anomalies. *Phys Earth*, *4*, 3–19.

Serri, G., Innocenti, F., & Manetti, P. (2001). Magmatism from Mesozoic to Present: Petrogenesis, time-space distribution and geodynamic implications. In *Anatomy of an orogen: The Apennines and adjacent Mediterranean basins* (pp. 77–103). Springer Netherlands.

Stavrev, P., & Gerovska, D. (2000). Magnetic field transforms with low sensitivity to the direction of source magnetization and high centricity. *Geophysical Prospecting*, *48*(2), 317–340. https://doi.org/10.1046/j.1365-2478.2000.00188.x

Trua, T., Serri, G., Marani, M., Renzulli, A., & Gamberi, F. (2002). Volcanological and petrological evolution of Marsili Seamount (southern Tyrrhenian Sea). *Journal of Volcanology and Geothermal Research*, *114*(3–4), 441–464. https://doi.org/10.1016/s0377-0273(01)00300-6

Trua, T., Serri, G., & Rossi, P. L. (2004). Coexistence of IAB-type and OIB-type magmas in the southern Tyrrhenian back-arc basin: Evidence from recent seafloor sampling and geodynamic implications. *Memorie Descrittive della Carta Geologica d'Italia*, *44*, 83–96.

Ventura, G., Milano, G., Passaro, S., & Sprovieri, M. (2013). The Marsili Ridge (Southern Tyrrhenian Sea, Italy): An island-arc volcanic complex emplaced on a 'relict' back-arc basin. *Earth-Science Reviews*, *116*, 85–94. https://doi.org/10.1016/j.earscirev.2012.11.005

Von Frese, R. R., Jones, M. B., Kim, J. W., & Kim, J. H. (1997). Analysis of anomaly correlations. *Geophysics*, *62*(1), 342–351. https://doi.org/10.1190/1.1444136

Von Frese, R. R. B., Hinze, W. J., & Braile, L. W. (1982). Regional North American gravity and magnetic anomaly correlations. *Geophysical Journal International*, *69*(3), 745–761. https://doi.org/10.1111/j.1365-246x.1982.tb02773.x

Woodward, D. J., & Mumme, T. C. (1993). Variation of magnetisation on White Island, New Zealand. *New Zealand Journal of Geology and Geophysics*, *36*(4), 447–451. https://doi.org/10.1080/00288306.1993.9514590

Wyering, L. D., Villeneuve, M. C., Wallis, I. C., Siratovich, P. A., Kennedy, B. M., Gravley, D. M., & Cant, J. L. (2014). Mechanical and physical properties of hydrothermally altered rocks, Taupo Volcanic Zone, New Zealand. *Journal of Volcanology and Geothermal Research*, *288*, 76–93. https://doi.org/10.1016/j.jvolgeores.2014.10.008

Zuo, B., Hu, X., Cai, Y., & Liu, S. (2019). 3D magnetic amplitude inversion in the presence of self-demagnetization and remanent magnetization. *Geophysics*, *84*(5), J69–J82. https://doi.org/10.1190/geo2018-0514.1